Design-oriented assessment of the residual post-fire bearing capacity of precast fiber reinforced concrete tunnel linings

Ramoel Serafini [a,b,*], Sérgio R.A. Dantas [a,b], Ronney R. Agra [a,b], Albert de la Fuente [c], Antonio F. Berto [b], Antonio D. de Figueiredo [a]

[a] Department of Civil Construction Engineering, Polytechnic School of the University of São Paulo, Avenida Professor Almeida Prado, Travessa 2, 83, 05424-970, São Paulo, Brazil
[b] Institute of Technological Research, Avenida Professor Almeida Prado, 532, 05508-901, São Paulo, Brazil
[c] Department of Civil and Environmental Engineering, Polytechnic University of Catalonia, Jordi Girona, 1-3, 08034, Barcelona, Spain

ARTICLE INFO

ABSTRACT

This study presents a meso-scale experimental program and employs a numerical approach to determine the bearing capacity of steel fiber reinforced concretes (SFRC) tunnel linings after fire exposure. First, the effect of temperature on the mechanical properties of SFRC was determined through a refined experimental campaign. Additionally, the suitability of the bending test and the DEWS test to assess the post-fire tensile properties of the SFRC was verified. Then, a thermo-mechanical model was implemented to assess the changes in the bearing capacity of SFRC for tunnels built with TBM technology. Results show that the thermo-mechanical model properly estimated the temperature distribution and the mechanical properties as a function of the duration of fire (t) and depth (z). The bearing capacity of the SFRC segments exposed to the ISO 834 and HFC fire curves were comparable when the condition $t_{ISO} = 2\,t_{HFC}$ was satisfied. Additionally, a greater bearing capacity reduction was numerically observed when the compressive region of the cross-section is affected by fire. The results obtained aid in the definition of appropriate rehabilitation operations, classifying the degree of damage sustained by the structure, and provides a procedure for designers regarding the effect of fire on SFRC structures.

1. Introduction

Tunnel structures are key infrastructure elements that aim to facilitate the mobility of people and goods in modern civilization in which investments may be linked to the reduction in social inequality [1,2]. In the last decades, the production of precast segments for tunnels benefited greatly from the use of discrete steel fibers as partial or total substitution to the conventional rebars in reinforced concrete (RC) [3,4]. The major benefits are related to the improved economic competitiveness, efficiency, and corrosion resistance provided by the steel fibers [5, 6]. In this context, the investigation of the damage imposed by fire on steel fiber reinforced concretes (SFRC) is a topic that requires attention from the scientific community.

Special attention must be given to fire events in tunnel structures since these events may cause social and structural damage. The reduced compartment dimensions and unfavorable ventilation conditions of these structures result in aggravated fire events with severe heating rates

and greater temperature values than a surface fire [7]. Therefore, the investigation of the fire safety of tunnels has been driven by the unquantifiable cost associated with the loss of human lives and the high social and economic costs due to the repair and temporary closure of tunnels.

The majority of the mesoscale studies regarding SFRC under high temperature have focused on the evaluation of the compressive strength (f_c), elastic modulus (E_c), and tensile strength (f_{Ft}) of the composite [8–15]. Results show that the increase in temperature tends to negatively affect the compressive and elastic properties of the SFRC, although the increase in fiber content mitigates the reductions in f_c [10]. The reductions in f_{Ft} are comparable to those suffered by plain concrete [13–15], which occurs because the steel fibers are not engaged before the matrix cracks. A considerable lack of studies focused on the evaluation of the post-crack design parameters was found in literature [16–20], which is required to determine the bearing capacity of SFRC under fire exposure [21,22]. These parameters are key factors for the

current analytical and numerical models employed for the design of tunnel linings [23,24].

Although several progenitive full-scale experimental campaigns and numerical models have been developed for RC tunnel linings under fire [25–27], the studies related to SFRC tunnel linings are scarce in literature. A study published by Yan et al. [28] exposed a SFRC pre-cast segment to the hydrocarbon fire curve (HFC) and evaluated the influence of the loading conditions and the presence of lining joints in the global fire performance of the segments. Di Carlo et al. [29] proposed a numerical approach to assess the bearing capacity of SFRC precast segments based on a staggered analysis that detaches the thermal problem from the mechanical one. The model proposed determines the bearing capacity of the SFRC by calculating the distribution of mechanical properties in the cross-section considering a stress-block constitutive law, the temperature-dependent constitutive equation of SFRC, and the translational and the rotational equilibrium conditions.

In this context, the basic concept underlying this study was to propose a meso-scale experimental program and employ a numerical approach to determine the bearing capacity of tunnel linings during a fire event. A comprehensive experimental investigation was conducted aiming to determine the mechanical behavior of the SFRC after exposure to target temperatures. Later, the temperature distribution and mechanical changes in SFRC as a function of the depth in order to determine the contribution of the material to the bearing capacity of the segments. The post-crack design parameters of SFRC were determined for target temperatures ranging between 150 and 750 °C by means of the Double Edge Wedge Splitting (DEWS) test. Moreover, the classical bending test and the DEWS test were evaluated regarding their applicability for the post-fire evaluation of the SFRC. The experimental and numerical analyses were used to characterize the post-crack behavior of SFRC under fire exposure.

The experimental results were employed as input parameters for a thermo-mechanical numerical model to assess the bearing capacity of a SFRC tunnel. The aforementioned assessment was conducted based on the design parameters of a tunnel to be executed in the city of São Paulo (Brazil). Therefore, the experimental and numerical approach used in this study may serve as a designing tool to determine the structural safety of a tunnel affected by fire, while also providing resources to determine an adequate rehabilitation procedure.

2. Materials and methods

Fig. 1 illustrates the scheme adopted for the experimental program and numerical investigation. The experimental campaign was conducted using two different heating procedures. Oven-heated specimens were employed to assess the mechanical properties at target temperatures and the chemical/mineralogical changes ranging between 150 °C and 750 °C, while specimens exposed to fire were used to assess the temperature distribution as a function of time and the post-fire bearing capacity of the SFRC. This paper is part of a Ph.D. research project that aims to evaluate the effect of fire on SFRC structures. Therefore, a detailed description of the materials can be found at Serafini et al. [30]. For the convenience of the reader, a brief description of the materials used in this research is provided.

2.1. Materials

A cement type CEM I 52.5R and silica fume (98% SiO_2) were used as cementitious materials. River and artificial sand and two coarse granite aggregates were used to increase the particle packing and a polycarboxylate-based superplasticizer was used to provide workability to the mix. The concrete matrix was reinforced using a commercial hooked-end steel fiber. Polypropylene microfibers were added to the mix to minimize the risk of explosive spalling during the fire test. Table 1 shows the data provided by the manufacturers for both fiber types.

2.2. Composition and preparation of SFRC

The SFRC mix design adopted was as close as possible to the concrete mix used in the construction of the Subway Line 6 of the city of São Paulo, Brazil (see Table 2). Contrary to real production conditions, no heat curing was employed for the SRFC due to the technical limitations on a laboratory scale. The steel fiber content adopted was 0.45% of total

Table 1
Data provided by the manufacturers for both fiber types.

Characteristics	Hooked-end steel fiber	Micro-synthetic fiber
Length (mm)	60	12
Diameter (mm)	0.75	0.03
Aspect ratio (l/d)	80	Not provided
Specific weight (kg/m^3)	7850	910
Specific surface area (m^2/kg)	Not provided	147
Melting point (°C)	Not provided	165
Tensile strength (MPa)	1225	Not provided
Young modulus (GPa)	200	Not provided
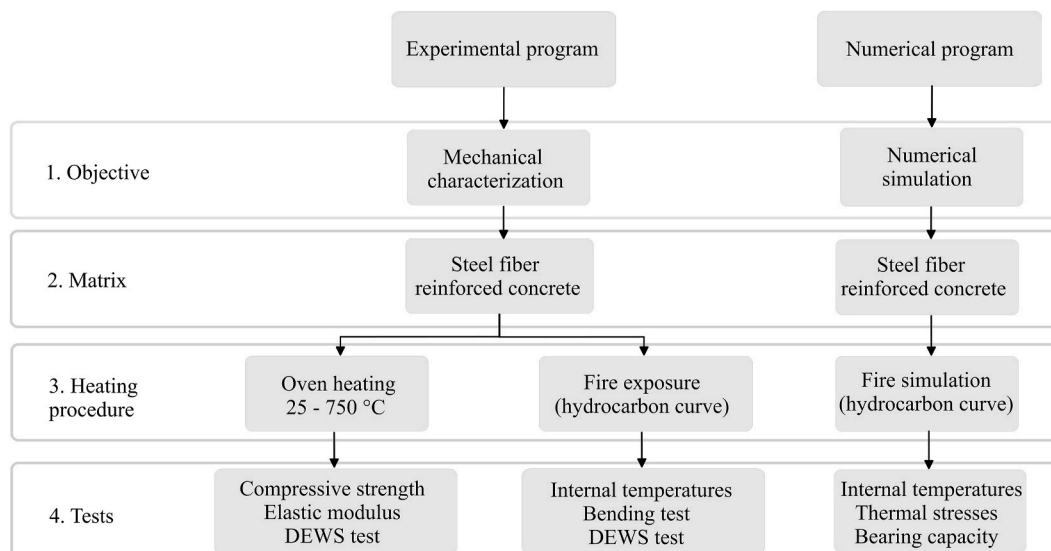
Fig. 1. Scheme adopted for the experimental and numerical programs.

Table 2
Materials necessary to fabricate one cubic meter of SFRC.

Materials	Dosage (kg/m^3)
Cement CEM I 52.5R	400
Silica fume	22
Water	165
Siliceous river sand	403
Artificial granite sand	269
Coarse granite aggregate - d$_{max}$: 19 mm	770
Coarse granite aggregate - d$_{max}$: 9.5 mm	330
Superplasticizer	3
Micro-synthetic fiber – anti-spalling	0.80
Hooked-end steel fiber	35

volume, which aimed to guarantee a minimum flexural bearing capacity, ductility, and crack control for the TBM jack's thrust phase [30]. The reinforcing fiber type adopted was a low-carbon cold-drawn steel fiber Dramix 3D RC-80/60-BG, with aspect ratio of 80, length of 60 mm, and tensile strength of 1225 MPa. The micro-synthetic fiber content was kept at 0.09% of total volume to mitigate the occurrence of explosive spalling, which was experimentally determined by the constructor specifically for the concrete mix and materials employed for the Subway Line 6.

The preparation of concrete followed the same methodology presented by Serafini et al. [30]. In the fresh state, the SFRC presented a specific weight of (2430 ± 52) kg/m^3 and a slump value of (50 ± 10) mm. During the casting procedure, thermocouples type K were inserted in one of the prismatic specimens in preset depths of 3, 6, 9, 12, and 15 cm from the surface exposed to fire. A total of 30 cylindrical specimens (Ø100 × 200 mm) and 20 prismatic specimens (150 x 150 × 550 mm) were cast, the latter being 7 prismatic specimens for bending test and 13 prismatic specimens that were cut into cubes (150 × 150 mm) for the DEWS test. The specimens were cured in a saturated room for the first 72 h after demolding, and later stored at room conditions (25 ± 1 °C) until the age of 150 days.

2.3. Heating procedures

This section describes the heating procedures adopted in this paper. Two main heating procedures were adopted: oven heated and fire exposure. After the heating procedure was conducted, all the specimens were cooled down and tested in post-cooling conditions.

2.3.1. Oven heating

An electric oven with maximum temperature capacity of 1000 °C and fix heating rate of (12 ± 2) °C/min was employed to heat cubic and cylindrical specimens. Specimens were heated at the temperatures of 150, 300, 450, 600, and 750 °C and kept at each temperature during 10, 8, 6, 4, and 4 h, respectively. The duration of the sustained thermal load was determined by numerical simulation based on the work of Carpio et al. [31] and had the objective to ensure uniform temperature of the specimens. After the heat exposure, the chamber was kept closed and cooling occurred during 24 h. Specimens that were not subjected to heating were used for comparative purposes.

2.3.2. Fire exposure

The exposure of specimens to fire was conducted in a vertical fire simulator at the Laboratory of Explosion and Fire Safety (LSFEx) from the Institute of Technological Research (IPT). Thermocouples were installed inside prismatic specimens during casting at distances of 3, 6, 9, 12, and 15 cm from the surface affected by fire. The fire curve was controlled by thermocouples installed at the surface of the prismatic specimens inside the fire simulator. A more detailed description and illustration of the equipment and the procedure adopted for the test is described in Serafini et al. [30]. A total of eight prismatic specimens were positioned on a masonry structural wall and a single-face fire

exposure was induced. The heat regime adopted was the hydrocarbon fire curve (HFC), following the recommended curves for underground structures [32]. Fig. 2 shows the HFC compared to the experimental fire curve obtained in this study. The fire test was kept during 120 min and the chamber was kept closed during 24 h for the cooling of specimens after the fire test was finished. During the fire exposure, the temperature inside the SFRC was recorded by thermocouples connected to a data acquisition system every 30 s.

2.4. Mechanical characterization

Table 3 summarizes the mechanical tests performed in the experimental program. All the tests for mechanical characterization were conducted with specimens in post-cooling conditions. Analysis of variances (ANOVA) and Tukey tests were employed to evaluate the experimental results statistically.

2.4.1. Compressive strength and elastic modulus

The compressive strength (f_c) and elastic modulus (E_c) of the SFRC were determined following the procedure presented by Serafini et al. [30]. A total of thirty specimens were evaluated, being five for each target temperature. The compressive and elastic properties were not determined for specimens exposed to the fire test due to the wide range of mechanical properties induced by the unifacial heat exposure. Also, the occurrence of crushing and grinding on the surface directly exposed to fire would compromise the results obtained.

2.4.2. Three-point bending test

The bending tests were performed in a servo-hydraulic universal testing machine, INSTRON 8802, with a load cell of 250 kN and in closed-loop configuration. The Crack Mouth Opening Displacement (CMOD) was controlled in accordance with the rates defined by the EN 14651 standard [33] and the methodology provided by Serafini et al. [30] using a knife-edge clip-gauge with maximum length of 4 mm. The flexural strength (f_j) for each given CMOD was calculated as:

$$f_j = \frac{3F_j.l}{2bh_{sp}^2} \tag{1}$$

Where F_j is load at a given CMOD (in N); l is the span (in mm); b is the
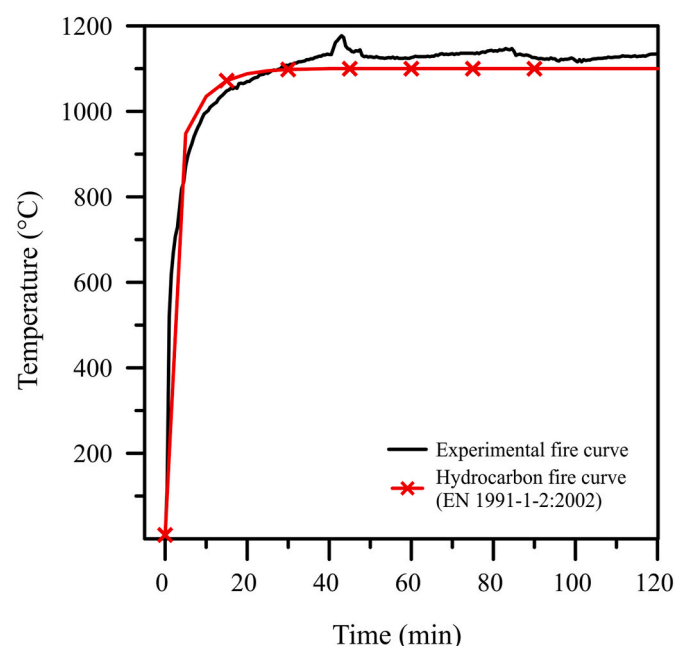
Fig. 2. Comparison between the HFC and the experimental fire curve.

Table 3
Summary of the mechanical tests conducted.

Test	Property	Specimen type	Heating procedure	Quantity
Compressive test	Compressive strength	Cylindrical	Oven heated $25 \leq T \leq 750$ °C	30
	Elastic modulus	Cylindrical	Oven heated $25 \leq T \leq 750$ °C	
DEWS test	Tensile properties	Cubic	Oven heated $25 \leq T \leq 750$ °C	30
	Tensile properties	Cubic	Fire test(HFC)	8
Bending test	Tensile properties	Prismatic	Fire test(HFC)	7

width of the specimen (in mm); and h_{sp} is the distance between the tip of the notch and the top of the specimen (in mm). The results obtained by the prismatic specimens at room temperature are also verified according to the procedure presented by the *fib* Model Code [34] regarding the verifications for the SFRC to be considered a structural material.

A total of seven prismatic specimens were tested under bending, being three SFRC prismatic specimens taken as reference and four prismatic specimens tested after fire exposure. The fire-exposed specimens were positioned in a way that the flexural tensile stresses were generated in the region closer to the fire (see Fig. 3). This setup was adopted to reduce the punching interaction in the region affected by fire, which also mitigates the occurrence of crushing and grinding interactions.

2.4.3. Double Edge Wedge Splitting (DEWS) test

The DEWS test was employed to assess the tensile properties of oven-heated and fire exposed cubic specimens. The test was performed following the simplified methodology presented by Borges et al. [35]. Cubic specimens with sides measuring 150 mm were produced by cutting the prismatic specimens. Since a mode I fracture is induced during the DEWS test, the influence of crushing or grinding of concrete during the test may be considered negligible [36].

The removal of cubic specimens and execution of the grooves/notches were conducted before the heating procedure for oven-heated specimens and after the heat procedure for fire-exposed specimens. This difference was adopted to mitigate the influence of lateral heating during the fire test, which is discussed in detail in Serafini et al. [30]. For the fire-exposed specimens, the triangular grooves were cut along two

Fig. 3. The three-point bending test setup for specimens exposed to fire.

opposite sides of the cubes in the face positioned 90° from the face exposed to fire and respecting the same orientation as the oven-heated specimens. Fig. 4 illustrates the DEWS test setup for specimens exposed to fire.

Steel plates with thickness of 0.9 mm were glued to the surface of the grooves and graphite powder was used to lubricate the contact between the roller and the plates. This procedure results in reduced frictional interaction in the roller-specimen contact [37]. The tensile strength of the matrix (f_{Ft}) and the post-crack tensile strengths related to serviceability (f_{Fts}) and the ultimate limit state (f_{Ftu}) were determined based on the results. The crack-opening displacement (COD) of 0.25 and 1.25 mm were adopted to determine the f_{Fts} and f_{Ftu} values since they are representative of the serviceability (SLS) and ultimate limit state (ULS) conditions [35]. A total of five prismatic specimens were employed for each target temperature in the oven-heated scenario, while eight cubic specimens were employed for the post-fire scenario.

2.4.4. Coefficient of mechanical degradation

The coefficient of mechanical degradation is a factor calculated based on experimental results that can be applied to reduce the bearing capacity of the layers of SFRC in a structure, as described by the Italian guideline CNR-DT 204 [38]. This coefficient has a particular use for the assessment of fiber reinforced concrete structures by means of cross-sectional analysis [38,39]. The results obtained during the mechanical characterization of oven-heated specimens were used to calculate the coefficient of mechanical degradation for the compressive strength (K_c), tensile strength (K_{Ft}), elastic modulus (K_{Ec}), and the post-crack tensile strength relative to a COD of 1.25 mm (K_{Ftu}).

The oven-heated results of K_c and K_{Ftu} were chosen to be analyzed since they represent the most important parameters at the ULS condition for SFRC structures. In this sense, the oven-heated results of K_c and K_{Ftu} were paired with the internal temperature distribution calculated by the thermal model to estimate the differential damage due to fire as a function of z and t. The results obtained were compared to the results employing the analytical curve proposed by the Italian guideline CNR-DT 204 [38].

2.5. Numerical simulation

The numerical model first developed by Di Carlo et al. [29] and later reproduced and refined by Carpio et al. [40] was employed. The main aspects related to the numerical model employed are briefly discussed in this paper for the convenience of the reader.

The exposure of concrete to a fire event results in a non-linear distribution of temperatures and affects the physical, thermal, and mechanical properties of the material. In this context, the numerical model solves the thermal problem by means of finite difference method (FDM) applied to the Fourier heat transfer equation. The net heat flux transferred from the fire source to the SFRC surface is determined considering the heat transferred by convection and radiation. The changes in specific heat, density, and thermal conductivity as a function of temperature followed the constitutive equations presented in the EN 1992-1-2:2004 [39].

The thermal model calculates the temperature distribution as a function of time inside the SFRC cross-section, which serves as input for the mechanical problem. Thus, the numerical model adopts a staggered analysis that detaches the thermal problem from the mechanical one. The mechanical problem is solved by considering the temperature-dependent constitutive equation of the material. The stress-strain distribution in the cross-section was calculated based on the non-compliance between the thermal strains and the kinematic requirements of the total strain field imposed by the Navier-Bernoulli hypothesis, as described in detail in Carpio et al. [40]. Lastly, the bearing capacity of the SFRC specimens was evaluated by calculating the distribution of compressive and tensile strength in the cross-section considering a stress-block constitutive law, the temperature-dependent
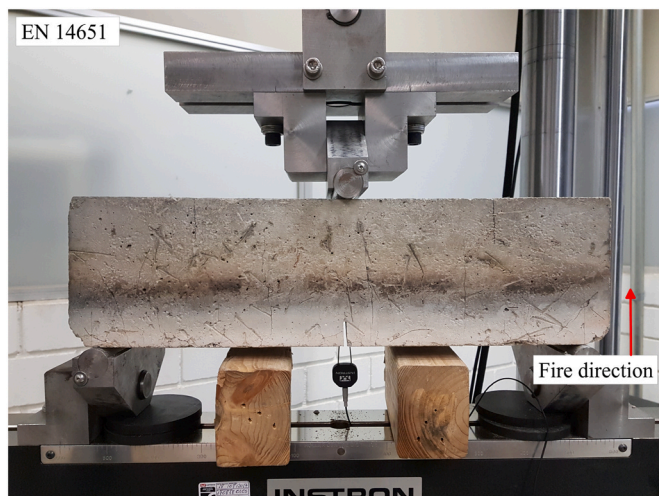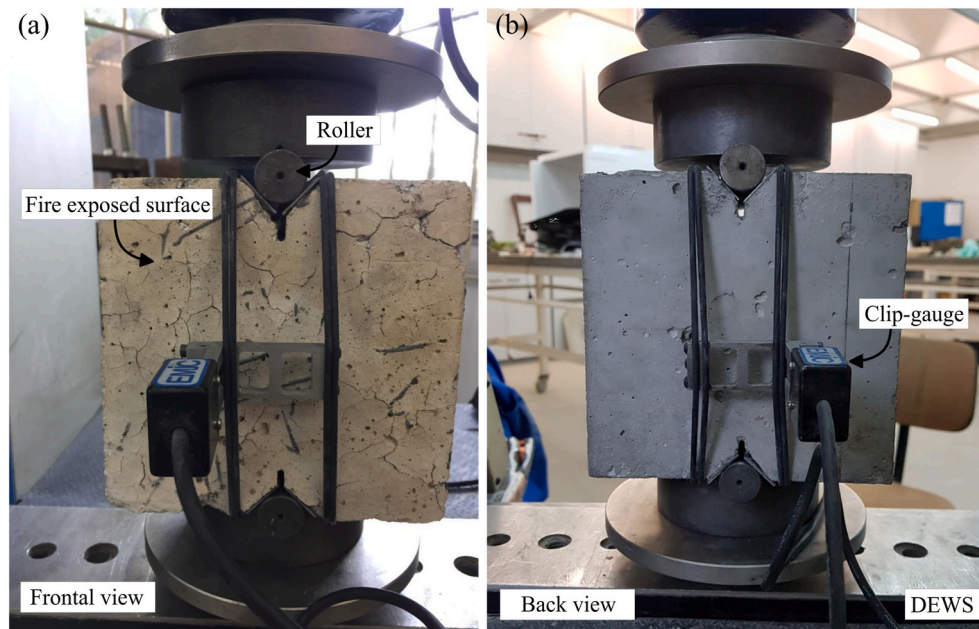
Fig. 4. The (a) frontal view and (b) back view of the DEWS test setup for specimens exposed to fire.

constitutive equation of SFRC, and the translational and the rotational equilibrium conditions as shown by Di Carlo et al. [29].

The numerical simulation was conducted considering a SFRC density of 2400 kg.m^{-3}, specific heat of 900 J.kg^{-1} K^{-1}, thermal conductivity of 1.2 W.m^{-1} K^{-1}, emissivity of 0.9, convective coefficient of 25 W.m^{-2} K^{-1}, initial temperature of 20 °C, and a specimen height of 150 mm. Also, the mechanical properties of the SFRC were inputted as $f_c = 83.9$ MPa, $f_{LOP} = 6$ MPa, $f_{R1} = 4.3$ MPa, and $f_{R3} = 3.0$ MPa. The average values were used in this simulation in order to better represent the behavior of the material in the meso-scale, and are not employed for design purposes. Moreover, the experimental values of K$_c$ and K$_{Fft}$ were used as input and linearly interpolated in during the numerical simulation. The fire simulation was conducted considering the HFC with the heating procedure applied to the bottom side of the specimen. The aforementioned values and procedures were adopted aiming to better simulate the concrete experimentally tested in this study.

3. Results and discussion

3.1. Oven-heated mechanical properties

Fig. 5 shows the coefficients of mechanical degradation for the compressive and tensile properties compared to European standards. The SFRC produced had a f_c of (83.9 ± 0.6) MPa and an E_c of (36.3 ± 0.5) GPa at the age of 150 days. In the temperature range between 150 and 750 °C, the f_c reduced between 6.3% and 97.7%, while the E_c reduced between 24.6% and 99.7% when compared to room temperature results. The K_c and K_{Ec} values obtained in this study were significantly lower than the values presented by the Eurocode, which may be a result of the superposition of several factors. The first is the increased porosity due to the ignition of micro-synthetic fibers, which results in pores that mitigate thermal spalling at the cost of reductions in compressive strength [36]. Secondly, the differences in the heat regimes employed, since depending on the specimen dimensions and the distribution of the specimens in the oven (*e.g.* closely packed) may not truly result in an homogeneous distribution of temperature. And lastly, the European curves are based on cubic specimens that tend to yield lower reductions in terms of compressive strength than cylindrical ones [41]. Even with those considerations, the K_c and K_{Ec} values are in line with similar studies found in literature [42–44].

A severe reduction in E_c between the temperatures of 150 and 450 °C was observed, which may be attributed to changes in the volume of solids associated to the changes in the pore structure of the matrix [45], the degradation of micro-synthetic fibers [30], and changes in the porosity of aggregates [46]. These factors are also summed to the micro-crack formation in the interfacial transition zone between aggregates and the matrix and the considerable dehydration of hydrated products, which are known to influence the f_c and E_c of the composite [46].

In the temperature range between 150 and 750 °C, the f_{Ft} reduced between 12.3% and 96.8% and the f_{Ftu} reduced between 15.9% and 99.2% when compared to room temperature results. For temperatures up to ~450 °C the reductions in f_{Ft} were more drastic than those in f_{Ftu}. This difference arises from the considerable effect imposed by the dehydration of the cement paste and the thermal-induced cracks on the f_{Ft} [46], while the f_{Ftu} is governed by the bond-slip mechanism of the steel fibers. Therefore, the reductions in terms of f_{Ftu} tend to be lower than those obtained for f_{Ft}, especially since the bond-slip mechanism of steel fibers is not significantly affected up to ~400 °C [47–51]. Additionally, the K_{Ft} and K_{Ftu} results agree well with the curve presented by the Italian guideline, CNR-DT 204 [38], as well as with the results obtained by bending tests in literature for a similar class of SFRC [17–19].

3.2. Post-fire results

3.2.1. Qualitative physical evaluation

Fig. 6 illustrates the physical changes that occurred on the prismatic specimens after fire exposure. The occurrence of explosive spalling did not occur in any of the specimens tested in this study, which may be attributed to the micro-conduits (*i.e.* voids) created by the melting of micro-synthetic fibers in the concrete mix, as also observed by other researchers in literature [52,53]. Moreover, the average mass loss of SFRC prismatic specimens after fire exposure was of 5.7%, which agrees well with literature results since the amount of mass loss of siliceous concretes is relatively low, even for temperatures beyond ~600 °C [54, 55].

The visual inspection showed the formation of an oxide surrounding the steel fibers that were closer to the fire source. This oxide formation occurs because the oxidizing nature of the atmosphere favors the combination between oxygen and iron at high temperatures. This oxidation
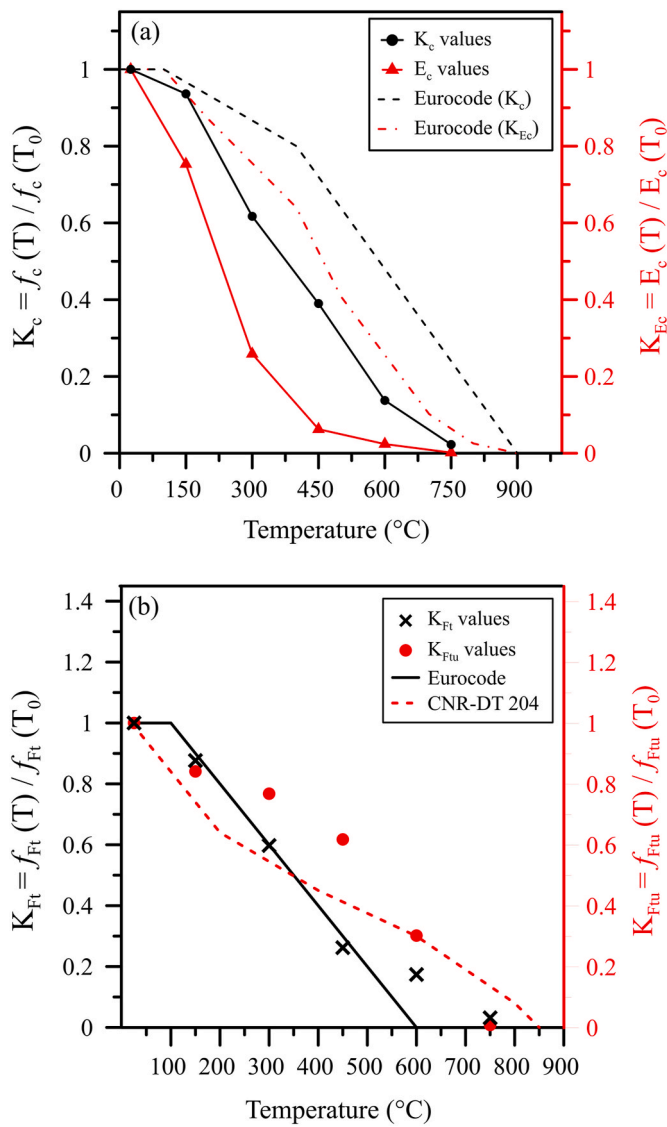
Fig. 5. Coefficients of mechanical degradation for the (a) compressive and (b) tensile properties compared to European standards.

process results in the formation of a three-layered scale structure that is friable and does not bring meaningful contribution to the mechanical properties of steel [56,57]. Also, the oxidation of steel fibers increases the total diameter of the fiber (oxide + steel) at the expanse of a reduction in the effective cross-sectional area for temperatures greater than ~750 °C [58]. Additionally, an extensive crack network may be

verified in the specimens. The extensive cracking verified is a result of the temperature-related deterioration and the non-uniform thermal related stresses generated by fire exposure [46]. Also, the more pronounced formation of cracks closer to the surface affected by fire may be attributed to the elevated temperatures recorded and the consequent degradation of the material.

3.2.2. Internal temperature distribution

Fig. 7 shows the experimental and numerical results for the internal temperature distribution in the SFRC as a function of z and t. It is possible to observe that the temperature inside the composite increases drastically for reduced values of z and greater values of t. The temperature readings inside the SFRC have recorded maximum values of 612, 403, 212, 141, and 112 °C for the z values of 3, 6, 9, 12, and 15 cm for $t =$ 120 min. In this sense, a wide range of temperatures is generated in the inner layers due to the low thermal conductivity of the composite, which is known to reduce even further with the increase in temperature [55, 59]. Moreover, the experimental temperature readings as a function of z and t show good agreement with the thermal model implemented.

The wide range of temperatures inside the SFRC resulted in a nonlinear distribution of thermal strains that do not comply with the kinematic requirements of the total strain field. This strain incompatibility generated compressive stresses at $z = 150$ mm and $z = 0$ mm, while
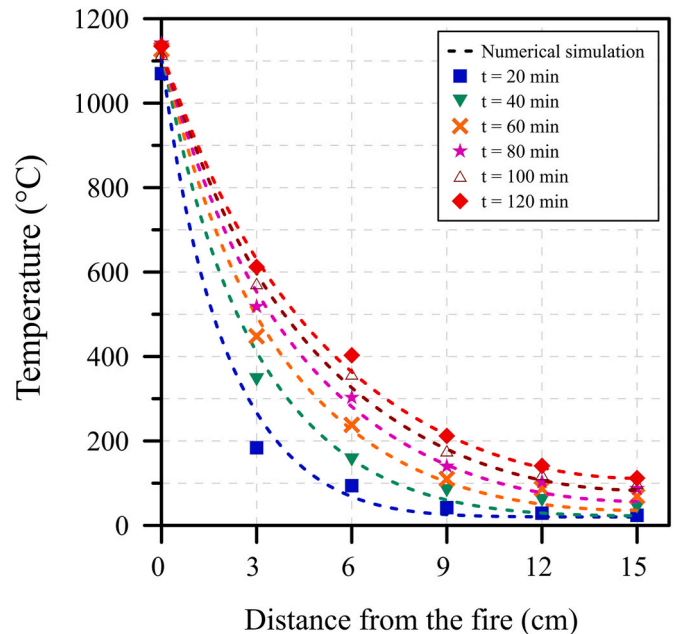
Fig. 7. Experimental and numerical results for the internal temperature distribution in the SFRC.

Fig. 6. Physical changes that occurred on the prismatic SFRC specimen after fire exposure.

tensile stresses arise in the central portion of the SFRC (see Fig. 8). At z = 0 mm, the compressive stresses reduce with the duration of fire due to the more rapid loss of mechanical strength caused by fire. The maximum compressive stress value of ~48 MPa occurred in the region closer to the fire for $t < 1$ min, which represents ~57% of the f_c. Such a considerable compressive stress occurred due to the high heating rate of the HFC and the fact that thermal-creep is not considered in the numerical model implemented [40,46].

Fig. 9 shows the temperature-time linear regression curves based on experimental results, as well as the internal heating rate values as a function of z. The results show that, at a given value of z, the temperature of the composite increases at a constant rate. This can also be observed by the almost constant offset between the temperature-depth curves in Fig. 7, especially for $z \geq 6$ cm. In this sense, the heating rate values calculated by the slope of linear regression curves for z equal to 3, 6, 9, 12, 15 cm were 4.84, 3.36, 1.63, 1.08, and 0.89 °C/min, respectively. Additionally, these internal heating rate values seems to increase logarithmically with the reduction in the values of z (see Fig. 9b).

The heating rate results obtained in this study agree well with previous results obtained with macro-synthetic fiber reinforced concrete (MSFRC) using the same concrete matrix tested in comparable conditions [30]. This result may indirectly suggest that the thermal conductivity of concrete is more significantly influenced by the properties of the concrete mix (*e.g.* aggregates, w/c ratio, binder type) than by the addition of fibers. Moreover, a study conducted by Liu et al. [59] shows that an increase of 1% in the steel fiber content added to the mix results in an increase of ~0.1 W/m.K in the thermal conductivity of SFRC, which is close to negligible when compared to the influence of other variables, such as type of aggregate, moisture conditions, and the test methodology adopted in experiments [60–62].

3.2.3. Differential damage in the SFRC

Fig. 10 shows the values of K_c and K_{Ftu} as a function of z and t compared to European standards. The K_c values determined based on experimental results for $t = 120$ min have reached 0.11, 0.52, 0.80, 0.87, and 0.95 for z values of 3, 6, 9, 12, and 15 cm, respectively. This means that the layers at $z \leq 3$ cm provide virtually no compressive strength to the SFRC, which is a result of the considerable dehydration, cracking,
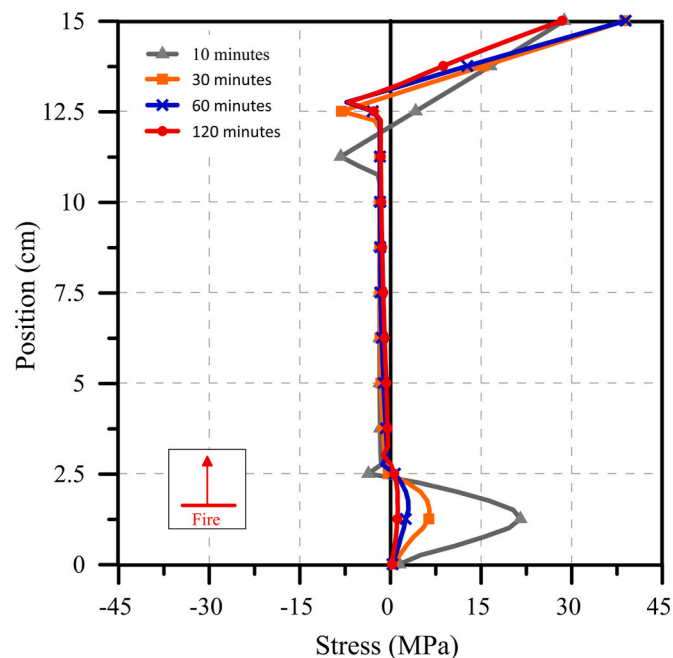
Fig. 8. Numerical simulation of the stress distribution in the SFRC as a function of fire duration.
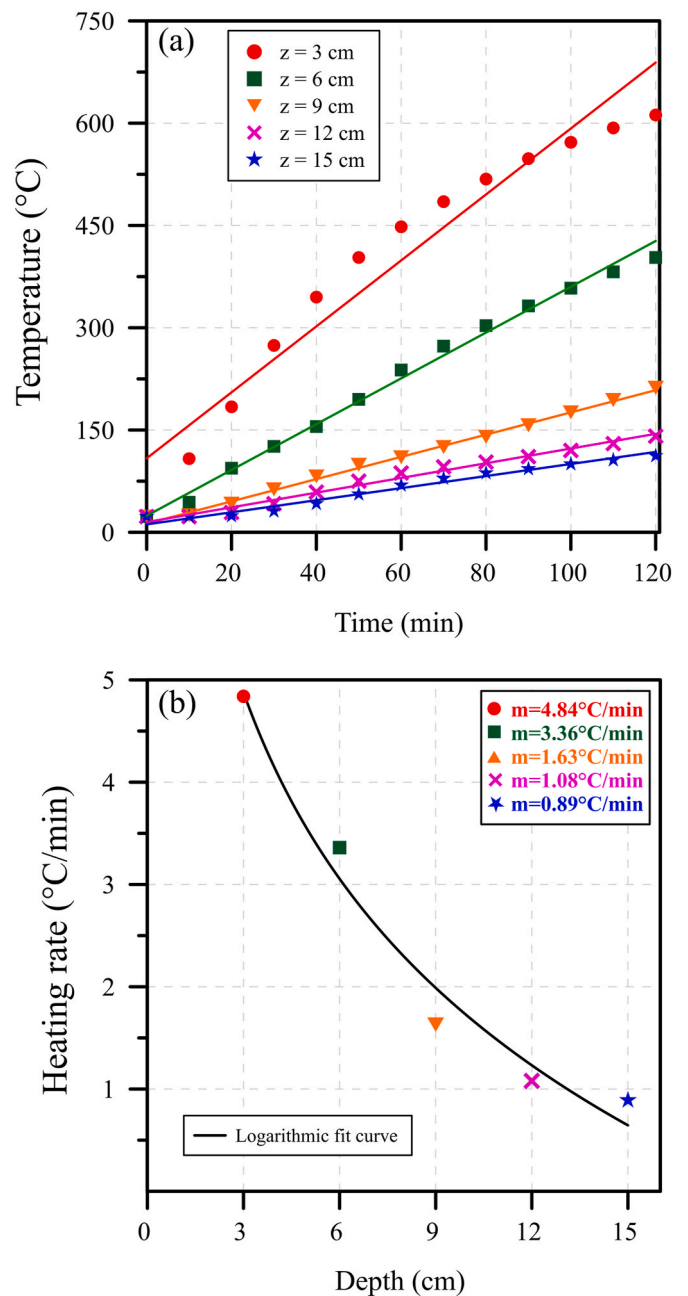
Fig. 9. (a) linear regression for the internal heating rate, and (b) internal heating rate values.

and deterioration that occurs in this region [30]. However, the K_c values ranged between 80% and 95% for $z \geq 9$ cm, which may suggest that layers at this depth can retain a considerable portion of the initial f_c value. Additionally, the K_c values are lower than those prescribed by Eurocode [39], as discussed in Section 3.1.

The values of K_{ftu} for $t = 120$ min have reached values of 0.24, 0.72, 0.82, 0.86, and 0.89 for z values of 3, 6, 9, 12, and 15 cm. These results suggest that the layers at $z < 3$ cm suffer a severe reduction in f_{Ftu} values, while layers at $z \geq 6$ cm may retain a significant portion of the initial f_{Ftu} value. The lower reductions observed for K_{Ft} compared to K_c can be attributed to the reduced effect of temperature on the bond-slip behavior of steel fibers up to ~400 °C [47–51] and, consequently, on the SFRC f_{Ftu} values. Moreover, the results obtained considering the K_{ftu} values presented by CNR DT-204 [38] have shown to be in favor of safety.

Also, the values of K_c and K_{Ftu} reduce non-linearly with the depth,
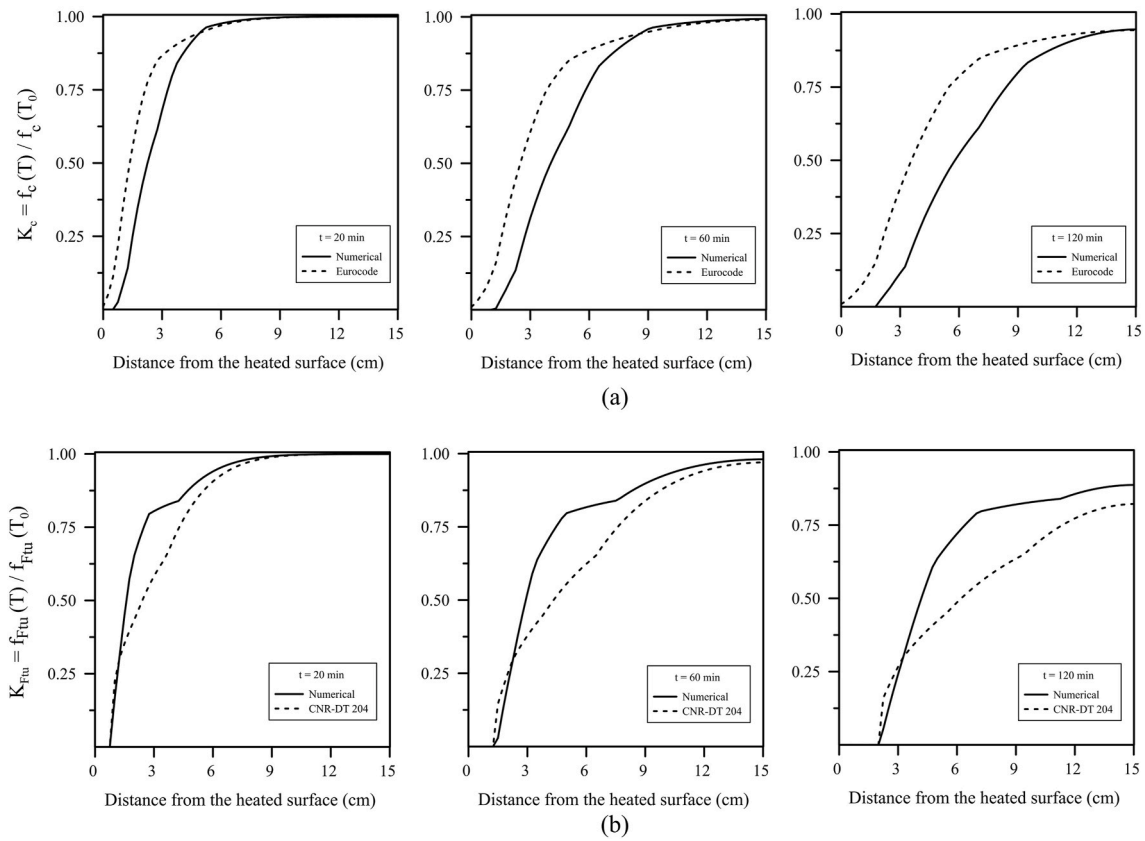
Fig. 10. Values of (a) K_c and (b) K_{Ftu} as a function of z compared to European standards.

which is directly proportional to the distribution of internal temperatures in the SFRC. However, the experimental results show that the reduction rate tends to be linear for a given value of z, as shown in Fig. 11. This feature may be noticed for K_c and K_{Ftu} for all the evaluated values of z, with exception of $z = 3$ cm for K_c. The non-linear changes in K_c at this specific value of z may be related to the aggressive heating rate provided by HFC and due to the proximity to the fire source. Moreover, the rate of reduction for K_{Ftu} in Fig. 11 seems to be lower than those for K_c, especially considering lower values of z. For every 60 min of fire exposure, the K_c reduced by 30.3%, 28.6%, 12.2%, 4.9%, and 3.1% and the K_{Ftu} reduced by 34.5%, 11.5%, 10.9%, 8.9%, and 6.9%, both for the respective z values of 3, 6, 9, 12, and 15 cm.

3.2.4. Bending test results

Fig. 12 shows the stress-CMOD curves for the SFRC before and after fire exposure by means of the three-point bending test. The SFRC tested at room temperature presented a softening behavior which is characteristic of composites with fiber contents lower than the critical fiber volume. In terms of post-crack parameters, the SFRC was classified as 4.0a ($f_{R1k} = 4.0$ MPa; slip softening) and met the minimum requirements at SLS (f_{R1}/f_{LOP}) and ULS (f_{R3}/f_{R1}) to be considered a structural material according to the methodology proposed by the *fib* Model Code 2010 [22].

The rupture peak associated with the matrix cracking is absent in specimens after fire exposure, which is justified by the extensive crack network induced by fire (see Section 3.2.1). The post-fire values of f_{LOP} and f_{R1} reduced by 88.9% and 40.1%, respectively, when compared with
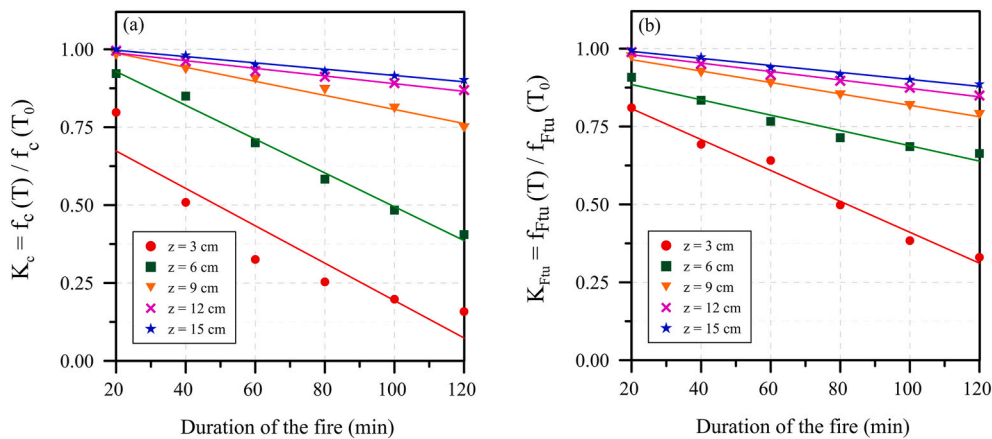
Fig. 11. Evolution of (a) K_c and (b) K_{Ftu} as a function of the duration of fire.
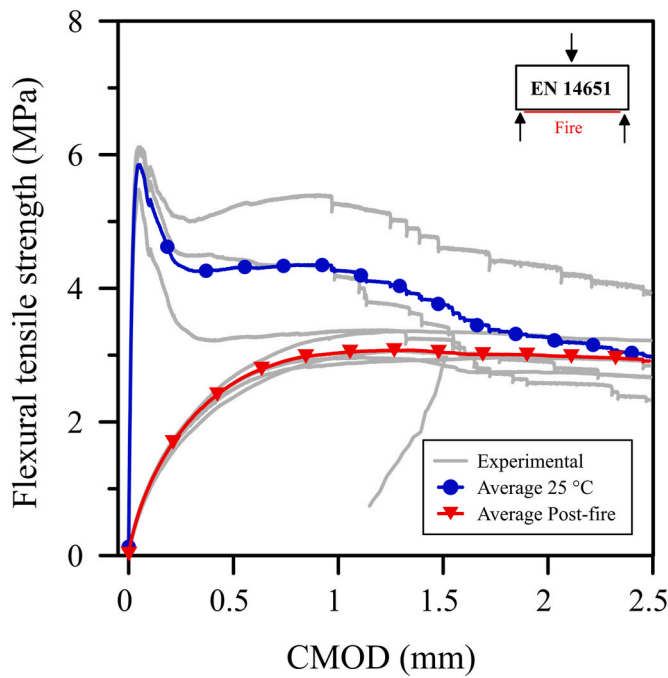
Fig. 12. Post-crack tensile strength for the SFRC before and after fire exposure by means of the three-point bending test.

reference specimens. Contrarily, f_{R3} and f_{R4} values did not show significant differences between the pre- and post-fire values, the slight differences observed being primarily due to the scatter of the bending test itself.

Moreover, the numerical simulation shows that the bearing capacity of the SFRC is slightly reduced when the fire affects the flexural tensile region of the specimens. Contrarily, a great reduction in the bearing

capacity is verified when the fire affects the compressive zone of the specimen (see Fig. 13). This occurs because the scalar value of f_c is greater than the scalar value of f_{Ftu}, therefore the temperature-related reductions in f_c tend to affect more significantly the bearing capacity of the cross-section. Secondly, the K_c is greater than K_{Ftu} for the same internal temperature value, which results in a more rapid loss of bearing capacity when the compressive region of the beam is heated.

This means that the results obtained by bending tests tend to be significantly influenced by the compressive portion of the cross-section, especially depending on the orientation of the prismatic specimens related to the surface affected by fire. Therefore, the bending test methodology adopted for the determination of post-fire f_{Ftu} may provide non-representative results of the actual properties of the composite after a fire event, while the investigation of alternative test methods is required. Moreover, the non-significant difference in results at CMOD = 2.5 mm may be influenced by the reduced effect of temperature on the bond-slip behavior of hooked-end steel fibers up to ~400 °C [47–51].

3.2.5. DEWS test

Fig. 14 shows the stress-COD curves before and after fire exposure and the comparison between oven-heated and fire-exposed specimens. The exposure to fire resulted in reductions of 71.4%, 66.7%, and 59.1% for f_{Ft}, f_{Fts}, and f_{Ftu}, respectively. These reductions may be attributed to the severe cracking caused by the dehydration of hydrated products in the cement paste [30], the temperature gradients induced by fire (see Section 3.2.1), and the temperature-related changes in the microstructure and the bond-slip mechanism of the steel fibers [51]. These macro- and microstructural changes are some of the factors that lead to the reduction in the tensile properties of the composite.

The post-fire tensile properties obtained by the DEWS test may be compared to the results obtained for oven-heated specimens, which were presented in Section 3.1. In this sense, a comparison between the post-fire stress-COD curves and the results for temperatures ranging between 150 °C and 750 °C are presented in Fig. 14b.

It is possible to observe that the post-fire f_{Ftu} values tend to the
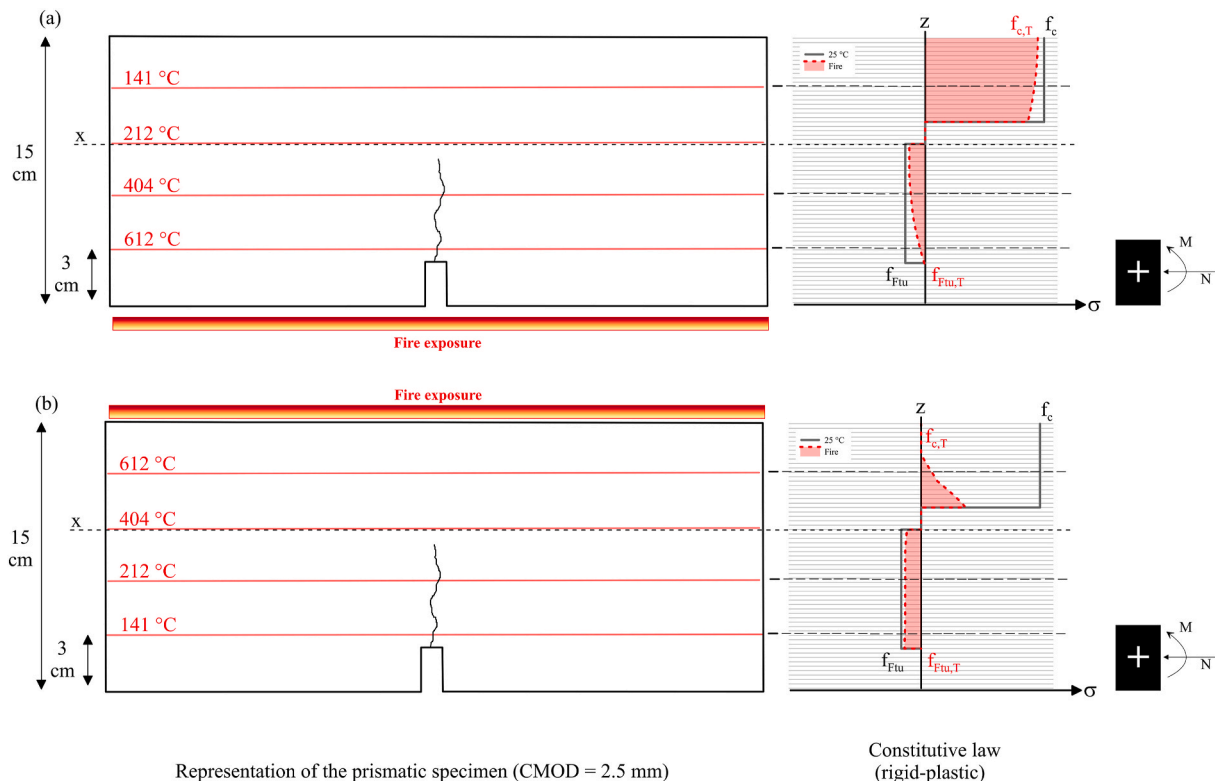
Fig. 13. Illustration of the bearing capacity under bending with fire effect on the (a) tensile region and (b) compressive region of the SFRC.
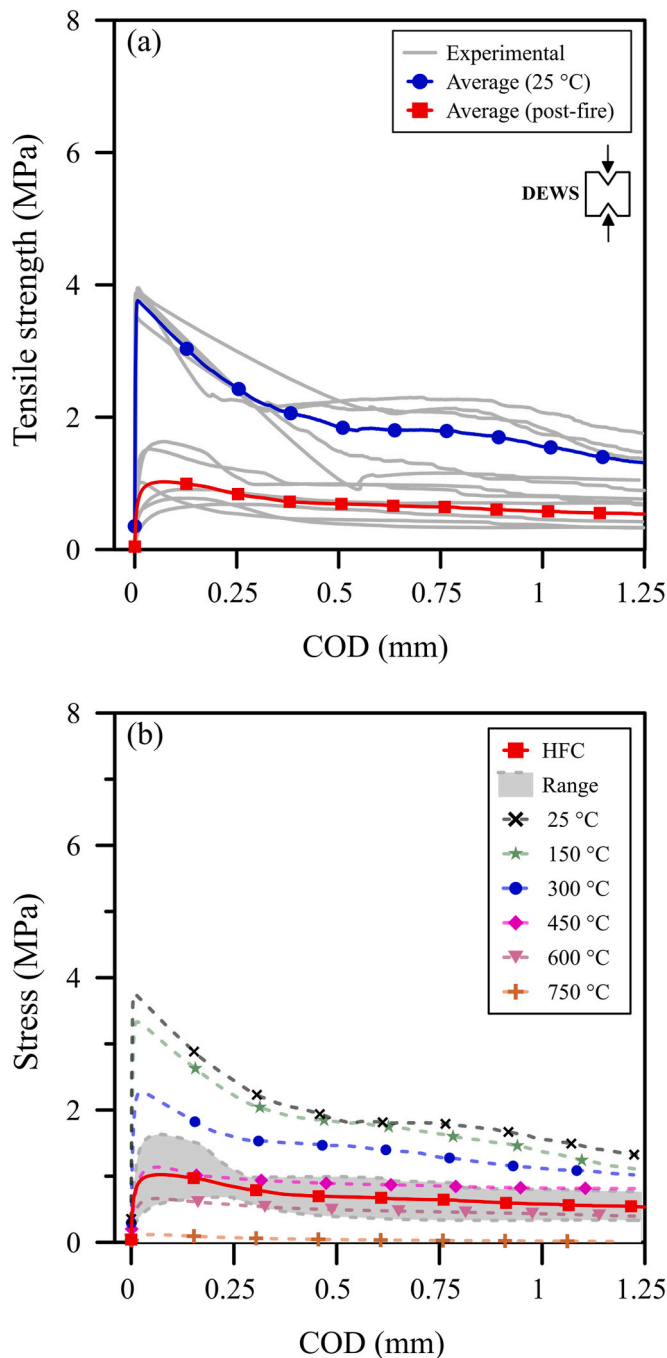
Fig. 14. Tensile properties after fire exposure compared to (a) room temperature and (b) oven-heated results.

average result obtained for temperatures between 450 °C and 600 °C. In this sense, the numerical simulation was employed as a tool to assess the distribution of f_{Ftu} in the cross-section as a function of z (see Fig. 15). The results show that the post-fire f_{Ftu} is null up to $z = 2$ cm and increases non-linearly up to 85.9% of the initial f_{Ftu} value with the increase in z. Therefore, the average post-fire f_{Ftu} value determined tends to represent the layers closer to the fire, which means that the DEWS test was capable of yielding more representative results than the EN 14651 bending test for the definition of f_{Ftu}.

4. Case study: São Paulo subway line

The numerical model implemented in this study was employed to assess the effect of a fire event on the bearing capacity of SFRC segments, taking as basis the design parameters of a tunnel to be executed in the city of São Paulo (Brazil). The steel fiber reinforced concrete law adopted is presented in Fig. 16, while the parameters employed in the numerical simulation are presented in Table 4. The values of f_{cd} and f_{R3d} were employed based on the design parameters considering a partial safety factor of $\gamma_F = 1.0$, since fire is an exceptional event. The numerical simulation was conducted considering the ISO 834 and the HFC. These fire curves were adopted to simulate two distinct scenarios with variable heating rate and maximum temperature. The bearing capacity of the cross-section was assessed by means of the Moment-Axial (M − N) interaction envelopes and the results are presented as a function of the fire curve adopted.

Fig. 17 shows the M − N interaction envelopes for the SFRC exposed to fire following the ISO 834 and the HFC. The results show that the exposure of the segments to an unifacial fire event resulted in a considerable loss in terms of bearing capacity. In this sense, the reductions in terms of bearing capacity have shown to be greater when the compressive region of the cross-section is closer to the fire (*i.e.* negative flexural moment). This occurs because the f_c represents a greater portion of the total bearing capacity of the segment, while the f_{Ftu} have lower scalar values. This effect was also observed both during the experimental campaign conducted and the numerical simulation, which was discussed in Section 3.2.4.

Even though the fire curves are different, it can be verified that the bearing capacity of SFRC is considerably reduced in both cases. The bearing capacity of the SFRC segments reduced more rapidly when exposed to the HFC, which is reasonable since the HFC prescribes higher values of maximum temperature and a rapid heating rate at the initial minutes of a fire. An interesting result is that the bearing capacity of the SFRC exposed to the ISO 834 and HFC fire curves were comparable when the condition $t_{(ISO)} = 2 \, t_{(HFC)}$ is satisfied (see Fig. 18). This condition was also verified in a parametric study conducted by Di Carlo et al. [29], which highlights the importance of determining the adequate fire curve for the proper assessment of tunnels exposed to fire events.

In this sense, the M − N interaction envelopes can be employed as useful tools to assess the cross-sectional stability of tunnels built with SFRC under fire exposure. In this particular case, the results presented in this section serve to the specific case of the Subway Line 6 at the city of São Paulo (Brazil). However, the tools presented in this study may be employed for the assessment of other tunnel structures built with SFRC. It is important to remind that validating the numerical simulation with experimental results is beneficial for a representative assessment of the bearing capacity of SFRC tunnel structures.

5. Conclusions

The following conclusions can be drawn from the present study:

- The temperature readings inside the SFRC exposed to fire reached 612, 403, 212, 141, and 112 °C for the z values of 3, 6, 9, 12, and 15 cm at $t = 120$ min. The distribution of temperatures obtained experimentally showed good agreement with the thermal model implemented. Moreover, the incompatibility between the thermal strains and the total strain field results in compressive stresses at $z = 0$ mm and $z = 150$ mm and tensile stresses at the central region of the specimens is subjected to fire.
- The reduction of the compressive (K_c) and post-crack tensile strength for a crack-opening of 1.25 mm (K_{ftu}) were determined as a function of temperature. The results in terms of K_c were lower than those prescribed by European guidelines, which was attributed to the melting of the micro-synthetic fibers and particularities of the heat regime adopted. Contrarily, the K_{ftu} values were greater than those prescribed by the CNR DT-204, which suggests that the guideline is on the safe side when micro-synthetic fibers are used and the explosive spalling is avoided.
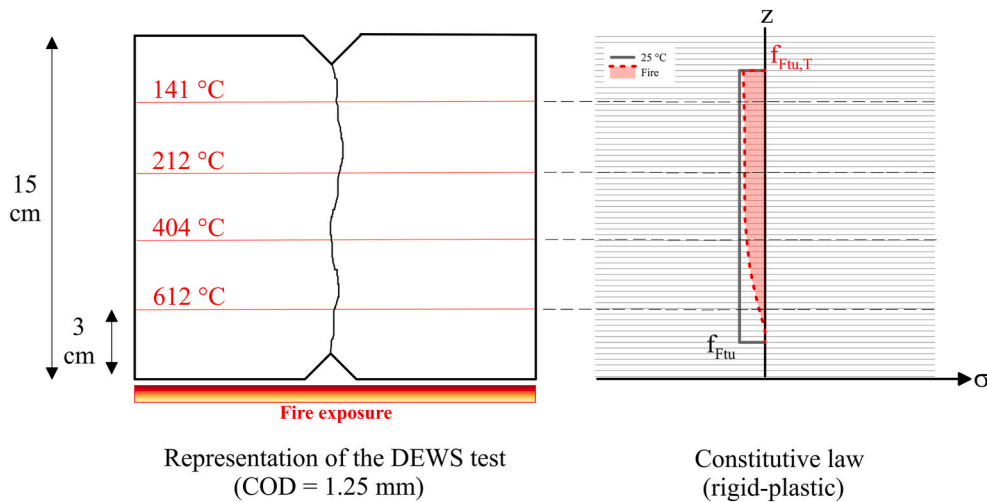
Fig. 15. Distribution of f_{Ftu} as a function of z for the DEWS test.
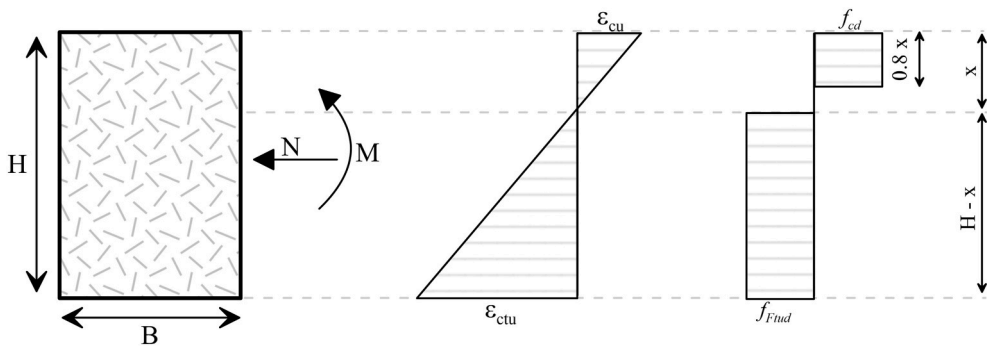
Fig. 16. Steel fiber reinforced concrete law adopted.

Table 4
Parameters adopted for the subway line numerical simulation.

Parameter	Input value
f_{cd} (MPa)	45
f_{R3d} (MPa)	3.0
f_{Ftud} (MPa)	1.0
H (in meters)	0.40
B (in meters)	1.0
Initial temperature (°C)	20
Emissivity	0.9
Density (kg.m^{-3})	2400
Specific heat (J.kg^{-1}.K^{-1})	900
Thermal conductivity (W.m^{-1}.K^{-1})	1.2
Convective coefficient (W.m^{-2}.K^{-1})	25

- The K_c and K_{Ftu} results fed the numerical model implemented and the differential damage inside the SFRC was estimated. The K_c values for $t = 120$ min have reached 0.11, 0.52, 0.80, 0.87, and 0.95 for z values of 3, 6, 9, 12, and 15 cm, respectively. The values of K_{ftu} obtained for $t = 120$ min have reached values of 0.24, 0.72, 0.82, 0.86, and 0.89 for z values of 3, 6, 9, 12, and 15 cm, respectively. This means that the layers at z $\leq$ 3 cm provide virtually no mechanical contribution, while layers further away (*e.g.* values of z $\geq$ 6 cm) may retain over 80% of the initial mechanical property value.

- The post-fire tensile properties of the SFRC were assessed by the bending test and the DEWS test. The post-fire results obtained by means of the bending test showed a reduction of 88.9% and 40.1% in terms of f_{LOP} and f_{R1}, respectively. Contrarily, f_{R3} and f_{R4} values did not show significant differences between the pre- and post-fire

values. The post-fire results obtained by means of the DEWS test showed reductions of 71.4%, 66.7%, and 59.1% for f_{Ft}, f_{Fts}, and f_{Ftu}, respectively. In this sense, the results suggest that the bending test may not be adequate to determine the ULS post-crack tensile properties of the composite after a fire, while the DEWS test could yield more representative results.

- The effect of a fire event on the bearing capacity of the SFRC segments was assessed using the numerical model implemented in this study. The results show that the fire exposure resulted in a considerable loss in terms of bearing capacity, which have shown to be greater when the compressive region of the cross-section is closer to the fire (*i.e.* negative flexural moment). This occurs because the f_c represents a greater portion of the cross-sectional bearing capacity, especially for SFRC with strain-softening behavior such as the one employed in this study. Therefore, the M − N interaction envelopes can be employed as useful tools to assess the local stability of tunnels built with SFRC under fire exposure.

- The bearing capacity of the SFRC segments decreased more rapidly when exposed to the HFC than to the ISO 834 fire curve, which is reasonable since the HFC prescribes higher values of maximum temperature and a rapid heating rate. This highlights the importance of determining the adequate fire curve for the proper assessment of tunnels exposed to fire events, which can be estimated based on experimental and numerical programs. An interesting result is that the bearing capacity of the SFRC exposed to the ISO 834 and HFC fire curves were comparable when the condition $t_{ISO} = 2\, t_{HFC}$ was satisfied.

Therefore, the results obtained are capable of evaluating the changes
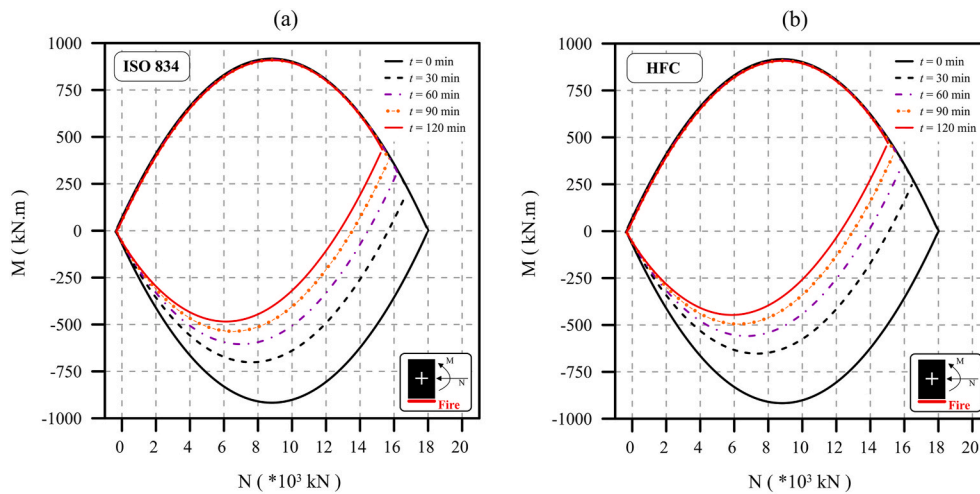
Fig. 17. The M − N envelopes for the SFRC exposed to fire following (a) the ISO 834 and (b) the HFC.
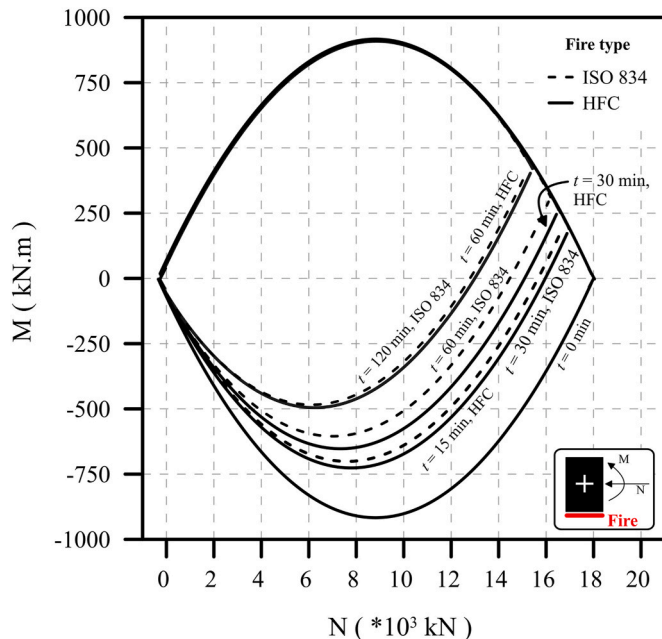
Fig. 18. Comparison between the M − N envelopes generated as a function of the fire curve adopted.

in temperature and in mechanical properties of SFRC in the cross-sectional level, as a function of space and time. More than that, the procedure proposed in this paper may be used as a tool to verify the stability SFRC tunnel linings in the design stage, as well as for structures affected by fire that require an adequate rehabilitation procedure. However, it is imperative to state that the validation of the model employed in this work must be conducted for full-scale simulation/testing in the future, especially considering that the heat transfer and structural response may be different due to thermal and deformation restraint conditions. Moreover, the results obtained in this paper are limited to the material specifications used in this study, which means that the M − N envelopes should not be generalized.

CRediT authorship contribution statement

Ramoel Serafini: Conceptualization; Methodology; Validation; Formal Analysis; Investigation; Data Curation; Writing – Original Draft; Visualization; Project administration. **Sérgio R.A. Dantas:** Methodology; Validation; Investigation; Data Curation; Writing - review & editing; Visualization; Project administration. **Ronney R. Agra:** Methodology; Validation; Investigation; Data Curation; Writing - review & editing; Visualization; Project administration. **Albert de la Fuente:** Methodology; Validation; Formal Analysis; Investigation; Writing - review & editing; Visualization. **Antonio F. Berto:** Validation; Resources; Writing - review & editing; Visualization; Supervision; Funding acquisition. **Antonio D. de Figueiredo:** Conceptualization; Methodology; Validation; Resources; Writing - review & editing; Visualization; Supervision; Funding acquisition.

Declaration of competing interest

The authors declare that they have no known competing financial interests or personal relationships that could have appeared to influence the work reported in this paper.

Acknowledgments

References

[1] D. Klenert, L. Mattauch, O. Edenhofer, K. Lessmann, Infrastructure and inequality: insights from incorporating key economic facts about household heterogeneity, Macroecon. Dyn. 22 (2018) 864–895, https://doi.org/10.1017/S1365100516000432.

[2] I. Josa, A. Aguado, Infrastructure, innovation and industry as solutions for breaking inequality vicious cycles, IOP Conf. Ser. Earth Environ. Sci. 297 (2019), 012016, https://doi.org/10.1088/1755-1315/297/1/012016.

[3] A. de la Fuente, A. Blanco, J. Armengou, A. Aguado, Sustainability based-approach to determine the concrete type and reinforcement configuration of TBM tunnels linings. Case study: extension line to Barcelona Airport T1, Tunn. Undergr. Space Technol. 61 (2017) 179–188, https://doi.org/10.1016/j.tust.2016.10.008.

[4] L. Liao, A. de la Fuente, S. Cavalaro, A. Aguado, Design of FRC tunnel segments considering the ductility requirements of the Model Code 2010, Tunn. Undergr. Space Technol. 47 (2015) 200–210, https://doi.org/10.1016/j.tust.2015.01.006.

[5] J.-L. Granju, S. Ullah Balouch, Corrosion of steel fibre reinforced concrete from the cracks, Cement Concr. Res. 35 (2005) 572–577, https://doi.org/10.1016/j.cemconres.2004.06.032.

[6] G.A. Plizzari, G. Tiberti, Steel fibers as reinforcement for precast tunnel segments, Tunn. Undergr. Space Technol. 21 (2006) 438–439, https://doi.org/10.1016/j.tust.2005.12.079.

[7] B. Yun, Operation systems in underground engineering, in: Undergr. Eng., Elsevier, 2019, pp. 239–259, https://doi.org/10.1016/B978-0-12-812702-5.00006-2.

[8] Y.-S. Tai, H.-H. Pan, Y.-N. Kung, Mechanical properties of steel fiber reinforced reactive powder concrete following exposure to high temperature reaching 800°C, Nucl. Eng. Des. 241 (2011) 2416–2424, https://doi.org/10.1016/j.nucengdes.2011.04.008.

[9] G.M. Chen, Y.H. He, H. Yang, J.F. Chen, Y.C. Guo, Compressive behavior of steel fiber reinforced recycled aggregate concrete after exposure to elevated temperatures, Construct. Build. Mater. 71 (2014) 1–15, https://doi.org/10.1016/j.conbuildmat.2014.08.012.

[10] O. Düğenci, T. Haktanir, F. Altun, Experimental research for the effect of high temperature on the mechanical properties of steel fiber-reinforced concrete, Construct. Build. Mater. (2015), https://doi.org/10.1016/j.conbuildmat.2014.11.005.

[11] C.-S. Poon, S. Azhar, M. Anson, Y.-L. Wong, Comparison of the strength and durability performance of normal- and high-strength pozzolanic concretes at elevated temperatures, Cement Concr. Res. 31 (2001) 1291–1300, https://doi.org/10.1016/S0008-8846(01)00580-4.

[12] C.S. Poon, Z.H. Shui, L. Lam, Compressive behavior of fiber reinforced high-performance concrete subjected to elevated temperatures, Cement Concr. Res. 34 (2004) 2215–2222, https://doi.org/10.1016/j.cemconres.2004.02.011.

[13] H. Li, G. Liu, Tensile properties of hybrid fiber-reinforced reactive powder concrete after exposure to elevated temperatures, Int. J. Concr. Struct. Mater. 10 (2016) 29–37, https://doi.org/10.1007/s40069-016-0125-z.

[14] W.Z. Zheng, H.Y. Li, Y. Wang, H.Y. Xie, Tensile properties of steel fiber-reinforced reactive powder concrete after high temperature, Adv. Mater. Res. 413 (2011) 270–276, https://doi.org/10.4028/www.scientific.net/AMR.413.270.

[15] D. Gao, D. Yan, X. Li, Flexural properties after exposure to elevated temperatures of a ground granulated blast furnace slag concrete incorporating steel fibers and polypropylene fibers, Fire Mater. 38 (2014) 576–587, https://doi.org/10.1002/fam.2198.

[16] A.C.S. Bezerra, P.S. Maciel, E.C.S. Corrêa, P.R.R. Soares Junior, M.T.P. Aguilar, P.R. Cetlin, Effect of high temperature on the mechanical properties of steel fiber-reinforced concrete, Fibers 7 (2019) 100, https://doi.org/10.3390/fib7120100.

[17] F.B. Varona, F.J. Baeza, D. Bru, S. Ivorra, Influence of high temperature on the mechanical properties of hybrid fibre reinforced normal and high strength concrete, Construct. Build. Mater. 159 (2018) 73–82, https://doi.org/10.1016/j.conbuildmat.2017.10.129.

[18] D. Choumanidis, E. Badogiannis, P. Nomikos, A. Sofianos, The effect of different fibres on the flexural behaviour of concrete exposed to normal and elevated temperatures, Construct. Build. Mater. 129 (2016) 266–277, https://doi.org/10.1016/j.conbuildmat.2016.10.089.

[19] M. Colombo, M. di Prisco, R. Felicetti, SFRC exposed to high temperature: hot vs. residual characterization for thin walled elements, Cement Concr. Compos. 58 (2015) 81–94, https://doi.org/10.1016/j.cemconcomp.2015.01.002.

[20] R.R. Agra, R. Serafini, A.D. de Figueiredo, Effect of high temperature on the mechanical properties of concrete reinforced with different fiber contents, Construct. Build. Mater. 301 (2021) 124242, https://doi.org/10.1016/j.conbuildmat.2021.124242.

[21] Serafini, et al., Mater. Struct. (2021), https://doi.org/10.1617/s11527-021-01819-2.

[22] Federation Internationale du Beton, in: Model Code for Concrete Structures 2010, Ernst & Sohn, Germany, 2013, p. 434.

[23] Z. Guan, T. Deng, G. Wang, Y. Jiang, Studies on the key parameters in segmental lining design, J. Rock Mech. Geotech. Eng. 7 (2015) 674–683, https://doi.org/10.1016/j.jrmge.2015.08.008.

[24] Guidelines for the design of shield tunnel lining, Tunn. Undergr. Space Technol. 15 (2000) 303–331, https://doi.org/10.1016/S0886-7798(00)00058-4.

[25] Z. Yan, H. Zhu, J. Woody Ju, W. Ding, Full-scale fire tests of RC metro shield TBM tunnel linings, Construct. Build. Mater. 36 (2012) 484–494, https://doi.org/10.1016/j.conbuildmat.2012.06.006.

[26] F. Yasuda, K. Ono, T. Otsuka, Fire protection for TBM shield tunnel lining, Tunn. Undergr. Space Technol. 19 (2004) 317, https://doi.org/10.1016/j.tust.2004.01.018.

[27] C. Pichler, R. Lackner, H.A. Mang, Safety assessment of concrete tunnel linings under fire load, J. Struct. Eng. 132 (2006) 961–969, https://doi.org/10.1061/(ASCE)0733-9445.

[28] Z. Yan, H. Zhu, J.W. Ju, Behavior of reinforced concrete and steel fiber reinforced concrete shield TBM tunnel linings exposed to high temperatures, Construct. Build. Mater. 38 (2013) 610–618, https://doi.org/10.1016/j.conbuildmat.2012.09.019.

[29] F. Di Carlo, A. Meda, Z. Rinaldi, Evaluation of the bearing capacity of fiber reinforced concrete sections under fire exposure, Mater. Struct. 51 (2018) 154, https://doi.org/10.1617/s11527-018-1280-2.

[30] R. Serafini, S.R.A. Dantas, R.P. Salvador, R.R. Agra, D.A.S. Rambo, A.F. Berto, A.D. de Figueiredo, Influence of fire on temperature gradient and physical-mechanical properties of macro-synthetic fiber reinforced concrete for tunnel linings, Construct. Build. Mater. 214 (2019) 254–268, https://doi.org/10.1016/j.conbuildmat.2019.04.133.

[31] J.M. Carpio, Numerical Model for the Thermo-Hygro-Mechanical Analysis of Concrete Elements from Early Ages, Universitat Politecnica de Catalunya, 2019.

[32] C.N. Costa, Dimensionamento de elementos de concreto armado em situação de incêndio, Universidade de São Paulo (2008), https://doi.org/10.11606/T.3.2008.tde-04092008-155911.

[33] En 14651, Test Method for Metallic Fibred Concrete — Measuring the Flexural Tensile Strength (Limit of Proportionality (LOP), Residual), United Kingdom, 2007.

[34] L. Liao, A. de la Fuente, S. Cavalaro, A. Aguado, Design procedure and experimental study on fibre reinforced concrete segmental rings for vertical shafts, Mater. Des. 92 (2016) 590–601, https://doi.org/10.1016/j.matdes.2015.12.061.

[35] L.A.C. Borges, R. Monte, D.A.S. Rambo, A.D. de Figueiredo, Evaluation of post-cracking behavior of fiber reinforced concrete using indirect tension test, Construct. Build. Mater. 204 (2019) 510–519, https://doi.org/10.1016/j.conbuildmat.2019.01.158.

[36] R. Serafini, R.R. Agra, R.P. Salvador, A. de la Fuente, A.D. de Figueiredo, Double edge wedge splitting test to characterize the design postcracking parameters of fiber-reinforced concrete subjected to high temperatures, J. Mater. Civ. Eng. 33 (2021), 04021069, https://doi.org/10.1061/(ASCE)MT.1943-5533.0003701.

[37] M. di Prisco, L. Ferrara, M.G.L. Lamperti, Double edge wedge splitting (DEWS): an indirect tension test to identify post-cracking behaviour of fibre reinforced cementitious composites, Mater. Struct. 46 (2013) 1893–1918, https://doi.org/10.1617/s11527-013-0028-2.

[38] CNR-DT 204, Guide for the design and construction of fibre-reinforced concrete structures, Ital. Natl. Res. Counc. (CNR), Rome, Italy (2007), https://doi.org/10.14359/10516.

[39] BS EN 1992-1-2, Eurocode 2 Design of concrete structures - Part 1-2: general rules-Structural fire design, Des. Concr. Struct. - Part 1-2 Gen. Rules-Structural fire Des (2004).

[40] J.M. Carpio, R. Serafini, D. Rambo, A. de la Fuente, A.D. De Figueiredo, Assessment of the bearing capacity reduction of FRC elements subjected to fire, in: Proc. Fib Symp. 2019 Concr. - Innov. Mater. Des. Struct., Kraków, Poland, 2019, pp. 1378–1386.

[41] R. Serafini, F.P. Santos, R.R. Agra, A. De la Fuente, A.D. de Figueiredo, Effect of specimen shape on the compressive parameters of steel fiber reinforced concrete after temperature exposure, J. Urban Technol. Sustain. 1 (2018) 10–20, https://doi.org/10.47842/juts.v1i1.7.

[42] A. Lau, M. Anson, Effect of high temperatures on high performance steel fibre reinforced concrete, Cement Concr. Res. 36 (2006) 1698–1707, https://doi.org/10.1016/j.cemconres.2006.03.024.

[43] B. Chen, J. Liu, Residual strength of hybrid-fiber-reinforced high-strength concrete after exposure to high temperatures, Cement Concr. Res. 34 (2004) 1065–1069, https://doi.org/10.1016/j.cemconres.2003.11.010.

[44] W. Zheng, H. Li, Y. Wang, Compressive stress–strain relationship of steel fiber-reinforced reactive powder concrete after exposure to elevated temperatures, Construct. Build. Mater. 35 (2012) 931–940, https://doi.org/10.1016/j.conbuildmat.2012.05.031.

[45] G.P. Alves, E.I. Jussiani, A.C. Andrello, B.M. Toralles, Effect of temperature rise on the microstructure of cementitious materials: a study through X-ray computed microtomography (μ-CT), Construct. Build. Mater. 237 (2020) 117446, https://doi.org/10.1016/j.conbuildmat.2019.117446.

[46] Z.P. Bažant, M.F. Kaplan, Concrete at High Temperatures: Material Properties and Mathematical Models, Longman, 1996.

[47] S. Abdallah, M. Fan, K.A. Cashell, Bond-slip behaviour of steel fibres in concrete after exposure to elevated temperatures, Construct. Build. Mater. 140 (2017) 542–551, https://doi.org/10.1016/j.conbuildmat.2017.02.148.

[48] S. Abdallah, M. Fan, D.W.A. Rees, Effect of elevated temperature on pull-out behaviour of 4DH/5DH hooked end steel fibres, Compos. Struct. 165 (2017) 180–191, https://doi.org/10.1016/j.compstruct.2017.01.005.

[49] S. Abdallah, M. Fan, K.A. Cashell, Pull-out behaviour of straight and hooked-end steel fibres under elevated temperatures, Cement Concr. Res. 95 (2017) 132–140, https://doi.org/10.1016/j.cemconres.2017.02.010.

[50] G. Ruano, F. Isla, B. Luccioni, R. Zerbino, G. Giaccio, Steel fibers pull-out after exposure to high temperatures and its contribution to the residual mechanical behavior of high strength concrete, Construct. Build. Mater. 163 (2018) 571–585, https://doi.org/10.1016/j.conbuildmat.2017.12.129.

[51] R. Serafini, R.R. Agra, L.A.G. Bitencourt, A. de la Fuente, A.D. de Figueiredo, Bond-slip response of steel fibers after exposure to elevated temperatures: experimental program and design-oriented constitutive equation, Compos. Struct. 255 (2021) 112916, https://doi.org/10.1016/j.compstruct.2020.112916.

[52] C. Maluk, L. Bisby, G.P. Terrasi, Effects of polypropylene fibre type and dose on the propensity for heat-induced concrete spalling, Eng. Struct. 141 (2017) 584–595, https://doi.org/10.1016/j.engstruct.2017.03.058.

[53] N. Yermak, P. Pliya, A.-L. Beaucour, A. Simon, A. Noumowé, Influence of steel and/or polypropylene fibres on the behaviour of concrete at high temperature: spalling, transfer and mechanical properties, Construct. Build. Mater. 132 (2017) 240–250, https://doi.org/10.1016/j.conbuildmat.2016.11.120.

[54] M.J. Hurley, D. Gottuk, J.R. Hall, K. Harada, E. Kuligowski, M. Puchovsky, J. Torero, JjM. Watts, C. Wieczorek, SFPE Handbook of Fire Protection Engineering, fifth ed., 2016, https://doi.org/10.1007/978-1-4939-2565-0.

[55] V. Kodur, Properties of concrete at elevated temperatures, ISRN Civ. Eng. 2014 (2014) 1–15, https://doi.org/10.1155/2014/468510.

[56] R.Y. Chen, W.Y.D. Yuen, Review of the high-temperature oxidation of iron and carbon steels in air or oxygen, Oxid. Metals (2003), https://doi.org/10.1023/A:1023685905159.

[57] H. Abuluwefa, The effect of oxygen concentration on the oxidation of low-carbon steel in the temperature range 1000 to 1250°C, Oxid. Metals (1996), https://doi.org/10.1007/BF01048639.

[58] R. Serafini, L.M. Mendes, R.P. Salvador, A.D. de Figueiredo, The effect of elevated temperatures on the properties of cold-drawn steel fibers, Mag. Concr. Res. (2020) 1–28, https://doi.org/10.1680/jmacr.19.00498.

[59] K. Liu, L. Lu, F. Wang, W. Liang, Theoretical and experimental study on multi-phase model of thermal conductivity for fiber reinforced concrete, Construct.

Build. Mater. 148 (2017) 465–475, https://doi.org/10.1016/j.conbuildmat.2017.05.043.

[60] K.Y. Shin, S.B. Kim, J.H. Kim, M. Chung, P.S. Jung, Thermo-physical properties and transient heat transfer of concrete at elevated temperatures, Nucl. Eng. Des. (2002), https://doi.org/10.1016/S0029-5493(01)00487-3.

[61] L. Phan, Fire performance of high-strength concrete: a report of the state-of-the-art, Fire Res (1996).

[62] V.K.R. Kodur, M.A. Sultan, Effect of temperature on thermal properties of high-strength concrete, J. Mater. Civ. Eng. (2003), https://doi.org/10.1061/(ASCE)0899-1561.